Correspondence

Fingerprint Classification Using an AM–FM Model

Marios S. Pattichis, George Panayi, Alan C. Bovik, and Shun-Pin Hsu

***Abstract*—Research on fingerprint classification has primarily focused on finding improved classifiers, image and feature enhancement, and less on the development of novel fingerprint representations. Using an AM–FM representation for each fingerprint, we obtain significant gains in classification performance as compared to the commonly used National Institute of Standards system, for the same classifier.**

***Index Terms*—AM–FM model, AM–FM transforms, fingerprint classification, multidimensional frequency modulation, probabillistic neural networks.**

I. Introduction

The problems of classifying and analyzing fingerprints is a difficult task which for a long time has required the service of trained experts [5], [11]. Indeed, fingerprint classification (ten- or single-print) continues to serve as a primary means of identification and record-keeping.

High-speed computing, database and networking technologies and sophisticated image processing methodologies have increased the topical significance of automatic fingerprint identification systems (AFIS), primarily for ten-print and single-print identification, which usually deploy optimal or adaptive classifiers, such as artificial neural networks (ANNs), to achieve reasonable classification results [1], [4], [6], [8], [9], [16]–[18].

Currently, no existing system uses physical models of the morphogenic processes giving rise to the fingerprint pattern, relying instead on intuitive image features for classification purposes. One possible approach that has been suggested is to view fingerprints as the solutions of reaction diffusion (RD) partial differential equations (RD-PDEs), which have been used to successfully describe biological morphogenesis and many natural pattern formations [10]. Unfortunately, the RD modeling problem is a very difficult inverse problem and we have seen no solutions to it. However, the solutions of RD equations often take the form of amplitude-modulated (AM) and frequency-modulated (FM) functions.

Here, we take the direct approach of modeling fingerprint images as AM–FM functions. Specifically, we propose the use of a computed FM image component to achieve improved fingerprint feature extraction, and hence, classification.

We begin by showing why AM–FM models are well-suited for describing fingerprints. Ridge variations are represented as an FM function, while variations in the ridge intensity modeled as an AM function. We show how the FM component can be isolated (by bandpass filtering) and extracted using a dominant component analysis algorithm (DCA). We then use the dominant FM component as input to the standard NIST fingerprint classification algorithm. We demonstrate significant classification performance improvement over a set of 200 NIST fingerprints.

Manuscript received March 15, 1999; revised February 26, 2001. This work was supported in part by the Air Force Office of Scientific Research Projects, Air Force Systems Command, USAF, under Grant F49620-93-1-9307.

M. S. Pattichis is with the Department of Electrical and Computer Engineering, University of New Mexico, Albuquerque, NM 87131-1356 USA (e-mail: pattichis@eece.unm.edu).

G. Panayi is with the Bank of Cyprus, Nicosia, Cyprus (e-mail: george.panayi@cisco.bankofcyprus.com).

A. C. Bovik and S.-P. Hsu are with the University of Texas at Austin, Austin, TX 78712 USA (e-mail: bovik@vision.ece.utexas.edu; shsu@ece.utexas.edu).

Publisher Item Identifier S 1057-7149(01)04471-2.

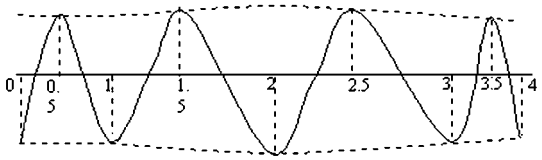

Fig. 1. Fingerprint image intensity variation along the ridge orientation coordinate (this is described by the ϕ_1-coordinate).

II. AM–FM Model for Fingerprint Images

We model the fingerprint image as a product $I(x_1, x_2) = a(x_1, x_2) f(\phi_1(x_1, x_2), \phi_2(x_1, x_2))$ where $a(x_1, x_2)$ denotes a slowly-varying amplitude function that is used to capture variations in the maximum (ridge peak) and minimum (ridge valley) fingerprint intensities. The new curvilinear coordinate system $(x_1, x_2) \rightarrow (\phi_1(x_1, x_2), \phi_2(x_1, x_2))$ is used for describing the image intensity variation along the ridge orientation $\phi_1(x_1, x_2)$, and the constant image intensity along the ridges $\phi_2(x_1, x_2)$. It is important to note that the two curvilinear coordinates introduced here will be continuous away from most minutiae points and corrupted ink areas. However, these discontinuities can be incorporated into the coordinate transformation. We will next comment on the curvilinear coordinate system, and use it to derive an AM–FM series expansion for the fingerprint.

Along the ϕ_2-coordinate curve, we expect that the image intensity of $I(x_1, x_2)/a(x_1, x_2)$ remains constant. We express the image intensity as only a function of the first curvilinear coordinate

$$f(\phi_1(x_1, x_2), \phi_2(x_1, x_2)) = f(\phi_1(x_1, x_2))$$

by abuse of notation. We note that we can always approximate $\phi_2(x_1, x_2)$ for any image by simply solving $I(x_1, x_2) = C$ for different values for C. For example, in ridge extraction, valleys are described by ϕ_2 coordinate curves for which $I(x_1, x_2) = C_{\min}$, while peaks are described by ϕ_2 coordinate curves for which $I(x_1, x_2) = C_{\max}$.

For the second set of coordinate curves, we consider ϕ_1-curves that are orthogonal to the ridge curves. By definition, a curve S is orthogonal to a set of coordinate curves, if at every image point the tangent vector of S is orthogonal to the tangent vector of the coordinate curve through the same point. In the NIST-standard, examples of such curves are computed by following the ridge orientation vectors. By definition, for any image, $\nabla I(x_1, x_2)$ will always be orthogonal to the $I(x_1, x_2) = C$ curves, and hence will approximate the ϕ_1-curves.

Along the ϕ_1-coordinate, we meet a peak, a valley, followed by another peak, a valley and so on. We assume that the peaks and valleys will recur at the some slowly-varying maximum and minimum intensity levels, where the amplitude function $a(x_1, x_2)$ is used to capture the variation (see Fig. 1). Under this assumption, we can provide the scale of the ϕ_1-coordinate to be proportional to the change in image intensity $\delta\phi_1 = \alpha\|\delta I\|$ for some constant α [12], [14]. For example, in wavelength units, the distance between a valley and a peak

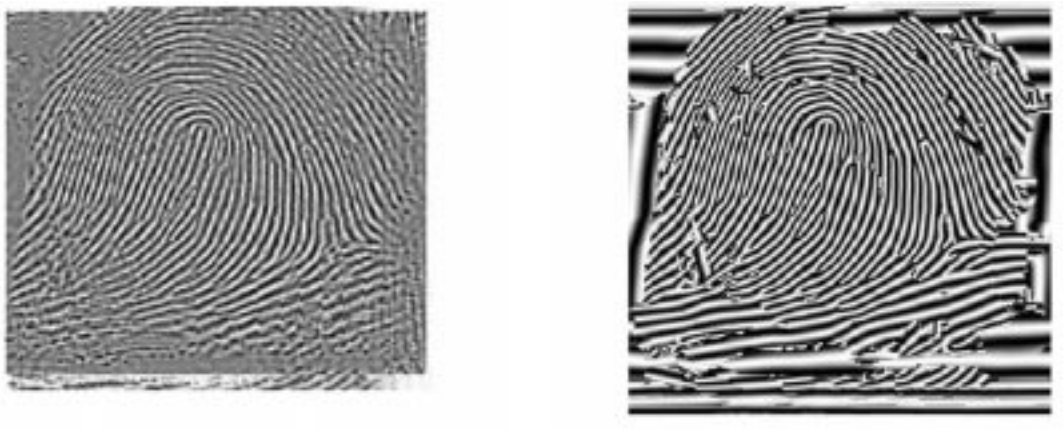

(a) (b)

Fig. 2. Comparison of the (a) NIST-enhanced fingerprint and (b) the fundamental FM component. It is clear that the fundamental FM component has much better defined ridges.

is 0.5, while the distance between any two valleys is 1. It is unrealistic to expect that the image intensity between peaks will follow a nice sinusoidal pattern. Instead, we only assume that the image intensity values repeat themselves from peak to peak, so that if $T = 2\pi$ denotes the normalized period, we have the important approximation: $f(\phi_1(x_1, x_2) + T) \approx f(\phi_1(x_1, x_2))$.

Using this approximation, we arrive at a Fourier series expansion approximation for f

$$f(\phi_1, \phi_2) \approx \sum_n H_n \exp[jn\phi_1].$$

Then, for $I(x_1, x_2)$, we have

$$I(x_1, x_2) \approx a(x_1, x_2) \sum_n H_n \exp[jn\phi(x_1, x_2)] \tag{1}$$

where the subscript has been dropped from the phase function. We note that examples of computing the coordinate transformation $(x_1, x_2) \rightarrow (\phi_1, \phi_2)$ and its inverse as described in this section have already been demonstrated in [12] and [14].

III. Isolating the Fundamental FM Component

If we let g denote the impulse response of a linear system, the system response $t(x_1, x_2)$ to an image expressed as a sum of AM–FM harmonics is approximately given by the quasi-eigenfunction approximation (QEA approximation) [2], [3], [7]

$$t(x_1, x_2) \cong a(x_1, x_2) \sum_n |G[n\nabla\phi(x_1, x_2)]| H_n \cdot \exp\{jn\nabla\phi(x_1, x_2) + \angle G[n\nabla\phi(x_1, x_2)]\} \tag{2}$$

where G denotes the Fourier transform of g, and $\angle$ denotes the angle argument symbol.

Hence, if most of the power in the fundamental AM–FM harmonic is concentrated in a circular disc of radii $\phi_{\min}$ and $\phi_{\max}$, we can use a bandpass filter to isolate the fundamental AM–FM component provided that $\phi_{\min} < \|\nabla\phi\| < \phi_{\max}$ and also $\phi_{\max} < \|n\nabla\phi\|$, $n > 1$. The requirement that the second inequality is satisfied over the entire fingerprint is overly restrictive. A much more realistic assumption is to require that the "local" power captured in the fundamental AM–FM component $H_1 a(x_1, x_2) G(\nabla\phi)$ is always higher than the power captured by any other harmonic $H_n a(x_1, x_2) G(n\nabla\phi)$, $n > 1$. Since we view the AM–FM series of (1) as the Fourier series of a prototype image undergoing a coordinate transformation, we note that the "local" power assumption is satisfied if the fundamental harmonic in the original Fourier series captures more energy than any other harmonic $|H_1| > |H_n|$, $n > 1$ (a very reasonable assumption that is expected to hold).

After visual inspection of the bandpass filter results for the first 20 NIST fingerprints, the radii for the bandpass filter were experimentally determined to be $\phi_{\min} = 0.25$ and $\phi_{\max} = 1.25$. For implementing the bandpass filter, the desired impulse response was set to the difference of the impulse response for a lowpass filter at $\phi_{\max} = 1.25$, and the impulse response of another lowpass filter at $\phi_{\min} = 0.25$. For the lowpass filters, we used

$$h(n_1, n_2) = \frac{R}{2\pi} \frac{J_1\left(R\sqrt{n_1^2 + n_2^2}\right)}{\sqrt{n_1^2 + n_2^2}}$$

where $h(n_1, n_2)$ denotes the impulse response for the first filter $R = \phi_{\min}$, the second filter $R = \phi_{\max}$, and J_1 denotes the Bessel function of the first kind.

Next, assuming that the "local" power assumption holds, we apply the DCA in order to estimate the phase of the fundamental FM harmonic: $\exp[j\phi(x_1, x_2)]$.

IV. Estimating the Fundamental FM Component

We now summarize the DCA [2], [7]. First, we apply a bandpass filter that removes the near-DC components. This is accomplished by 1) filtering the image with a lowpass filter that is supported within a circular disk centered at the origin of the frequency plane and 2) substracting the lowpass filtered image from the original image. We then proceed to the second step with the resulting image.

We apply a collection of Gabor (bandpass) channel filters $g_1, g_2, \ldots, g_M$ to the new image I, obtaining output images $t_1, t_2, \ldots, t_M$, satisfying $t_i = I * g_i$ where $*$ is convolution.

Let $G_1, G_2, \ldots, G_M$ denote the frequency responses of the Gabor channel filters. Using the Quasi-Eigenfunction Approximation (QEA), the filter outputs are approximately given by [2], [3], [7]

$$t_i(x_1, x_2) \cong a(x_1, x_2) \sum_n |G_i[n\nabla\phi_i(x_1, x_2)]| H_i \cdot \exp\{jn\nabla\phi_i(x_1, x_2) + \angle G_i[n\nabla\phi_i(x_1, x_2)]\}.$$

We obtain estimates for the instantaneous frequency

$$\nabla\phi_i(x_1, x_2) \cong \text{Real}\left\{\frac{\nabla t_i(x_1, x_2)}{j t_i(x_1, x_2)}\right\}$$

and the phase

$$\phi_i(x_1,\, x_2) \cong \arctan\left\{\frac{\text{Imaginary}\{t_i(x_1,\, x_2)\}}{\text{Real}\{t_i(x_1,\, x_2)\}}\right\}.$$

Using the instantaneous frequency estimate $\nabla\phi(x_1,\, x_2)$and the frequency response of the Gabor channel G_i, we estimate the amplitude

$$a(x_1,\, x_2) \cong \left|\frac{t_i(x_1,\, x_2)}{G_i(\nabla\phi(x_1,\, x_2))}\right|.$$

Having generated estimates for each channel filter, we next select a particular channel for each pixel. For each pixel, we select the channel with the maximum amplitude estimate

$$c_{\max}(x_1,\, x_2) = \arg\max_i\, a_i(x_1,\, x_2).$$

As we have explained, this channel is expected to capture contributions from the fundamental AM–FM harmonic only (no other harmonics). Then, the fundamental AM–FM component estimates are given by

$$\begin{aligned}\nabla\phi(x_1,\, x_2) &\cong \nabla\phi_{c\_\max}(x_1,\, x_2)\\ \phi(x_1,\, x_2) &\cong \phi_{c\_\max}(x_1,\, x_2)\\ a(x_1,\, x_2) &\cong a_{c\_\max}(x_1,\, x_2).\end{aligned}$$

The performance of the dominant component analysis algorithm has been studied quite extensively [2], [3], [7].

We display a typical FM component in Fig. 2. We note that all amplitude related ink variations have been eliminated. Also, due to the bandpass filtering, the background of the image appears as a low-frequency component. As we shall explain in Section V, for the purposes of fingerprint classification, there is no need to segment the low frequency components of the background from the actual fingerprint.

V. Fingerprint Classification Using the Fundamental FM Component

Fingerprint classification using PCASYS of the NIST consists of 1) feature extraction, followed by 2) feature classification. We will briefly describe each process separately (see [4] for more details).

To extract the fingerprint features, each fingerprint is first segmented and then enhanced. For performing the AM–FM fingerprint classification, we also used the NIST segmentation algorithm. However, instead of using the NIST-enhanced image, we used the fundamental FM harmonic. The fundamental FM harmonic $\exp[j\phi(x_1,\, x_2)]$ is estimated as explained in the preceeding section (using $M = 48$ Gabor filters).

The algorithm used by the NIST enhancer can be summarized in three steps [4]. First, partition the image into overlapping 32×32 pixel blocks, which are taken 24 pixels apart. Second, zero-out both low- and high-frequency components of the DFT spectrum, and modify the remaining DFT elements $\tilde{X}$ using: $\tilde{Y} = |\tilde{X}|^{0.3}\tilde{X}$. Third, evaluate the inverse DFT of $\tilde{Y}$ to get C, center the image pixels around the maximum value in C and rescale image intensity values to be in the range of zero to 255.

For comparison, the fundamental FM component and the NIST enhanced image are both shown for a typical fingerprint in Fig. 2. We note that small scars are removed from the FM image. However, over large noisy regions, phase estimates are erroneous; as demonstrated in the background regions of Fig. 2 (but see more recent results in [12] and [13]).

Notice that the FM image possesses clearly defined ridges, free of any ink variations. This facilitates the next step of estimating the orientation of each ridge. Furthermore, since the NIST algorithm estimates orientations throughout the fingerprint, there is no need to further segment the fundamental FM harmonic from its background.

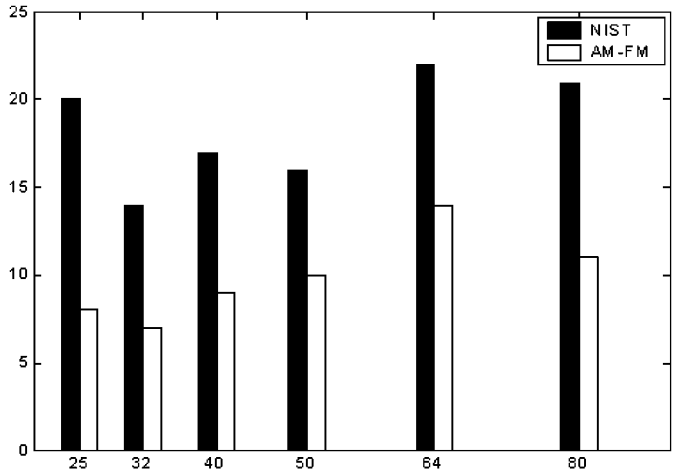

Fig. 3. Overall classification results for the NIST and the AM–FM methods. The first 100 NIST fingerprints were used for training, while the second set of 100 NIST fingerprints were used for testing the classifier. On the vertical axis, we plot the percentage of incorrectly classified fingerprints, while on the horizontal axis, we show how the number of components of the classification vectors that were used for the optimal smoothing factor β. Note that a smaller number of components capturing the fingerprint structure around the main fingerprint region is better than including a large number of components (which would surely capture the periphery of the fingerprints which is irrelevant to the classification problem).

Instead of using the NIST algorithm for estimating the orientations, we expect that if we used instantaneous frequency vector estimates, we would obtain more accurate estimates of the ridge orientations. Nevertheless, since orientation estimates are quantized to only eight quantization levels in a 30×28 array, we believe that the added accuracy is likely to be proven unnecessary.

We performed neural-net training based on orientations estimated on the FM images, and compared the fingerprint classification results against training and classification using orientations estimated from the original, NIST enhanced images. For reducing the number of classification vector components, a standard Karhunen–Loeve (KL) transform was used. For the KL transform, the sample covariance matrix of the full classification vectors is initially computed. Then, for using only n vector components, the n dominant eigenvalue/eigenvector pairs of the sample covariance matrix are computed. The mth vector component is set to the inner product between the full vector and the mth eigenvector.

For classification, we used a probabilistic neural network (PNN). The PNN falls within the category of nearest-neighbor classifiers [15], [4]. For a given vector $\mathbf{w}$ to be classified, an activation a_i is computed for each of the six classes of fingerprints ($i = 1,\, \ldots,\, 6$). The activation a_i is defined to be the total distance of $\mathbf{w}$ from each of the M_i prototype fingerprint vectors $\mathbf{x}_j^{(i)}$ that belong to the ith class

$$a_i = \sum_{j=1}^{M_i} \exp\left[-\beta\left(\mathbf{w} - \mathbf{x}_j^{(i)}\right)^T\left(\mathbf{w} - \mathbf{x}_j^{(i)}\right)\right]$$

where β is a smoothing factor. The normalized activations $\tilde{a}_i = a_i / \sum_{i=1}^{N} a_i$ provides a confidence estimate for the hypothesis that $\mathbf{w}$ belongs to class i. We then classify $\mathbf{w}$ into the class that yields the highest confidence. An important advantage of the PNN is that it provides confidence estimates for our classification decision. Also, to avoid dependence on the smoothing factor β, the value of β was set to the one that yielded the minimum misclassification error on the training set.

The results are summarized in Fig. 3. In all the examples, we used the first 100 fingerprints for feature extraction and training the NIST probabilistic neural network [15], and then used a second set of 100 different fingerprints for classification. The following six fingerprint classes are used in the classification

1) arch;
2) left loop;
3) right loop;
4) tented arch;
5) whorl;
6) scar.

The FM enhanced images consistently outperformed the NIST standard for all the different feature sets and all different learning rates that we have attempted. The performance improvements are significant, with the percent error for the FM algorithm approximately half of the corresponding error for the original NIST algorithm.

VI. Conclusion and Future Work

AM–FM models are well suited for fingerprint analysis and classification. We believe that future research on fingerprint classification will benefit from the use of AM–FM features. A variety of different AM–FM features have been investigated in [12], but the analysis still needs to be extended and proven on large fingerprint datasets. We believe that this paper demonstrated that taking this direction is indeed promising.

References

[1] J. L. Blue, G. T. Candela, P. J. Grother, R. Chellappa, and C. L. Wilson, "Evaluation of pattern classifiers for fingerprint and OCR applications," *Pattern Recognit.*, vol. 27, no. 4, pp. 485–501, 1994.

[2] A. C. Bovik, N. Gopal, T. Emmoth, and A. Restrepo, "Localized measurement of emergent image frequencies by Gabor wavelets," *IEEE Trans. Inform. Theory*, vol. 38, pp. 691–712, Mar. 1992.

[3] A. C. Bovik, J. P. Havlicek, M. D. Desai, and D. S. Harding, "Limits on discrete modulated signals," *IEEE Trans. Signal Processing*, vol. 45, pp. 867–879, Apr. 1997.

[4] G. T. Candela, P. J. Grother, C. I. Watson, R. A. Wilkinson, and C. L. Wilson, "PCASYS—A pattern-level classification automation system for fingerprints," Nat. Inst. Standards Technol., Tech. Rep. NISTIR 5647, Aug. 1995.

[5] Fed. Bureau Invest., *The Science of Fingerprints*. Washington, DC: U.S. Dept. Justice, 1984.

[6] U. Halici and G. Ongun, "Fingerprint classification through self-organizing feature maps modified to treat uncertainties," *Proc. IEEE*, vol. 84, pp. 1497–1512, 1996.

[7] J. P. Havlicek, "AM–FM image models," Ph.D. dissertation, Univ. Texas, Austin, 1996.

[8] A. K. Jain, "On-line fingerprint verification," *IEEE Trans. Pattern Anal. Machine Intell.*, vol. 19, pp. 302–314, Apr. 1997.

[9] K. K. Karu and A. K. Jain, "Fingerprint classification," *Pattern Recognit.*, vol. 29, no. 3, pp. 389–404, 1996.

[10] J. D. Murray, *Mathematical Biology*, 2nd ed. New York: Springer-Verlag, 1993.

[11] H. C. Lee and R. E. Gaensslen, *Advances in Fingerprint Technology*. Boca Raton, FL: CRC, 1994.

[12] M. S. Pattichis, "AM–FM transforms with applications," Ph.D. dissertation, Univ. Texas, Austin, 1998.

[13] M. S. Pattichis, A. C. Bovik, and M. D. Desai, "Latent fingerprint analysis using an AM–FM model," *Pattern Recognit.*, submitted for publication.

[14] M. S. Pattichis and A. C. Bovik, "AM–FM expansions for images," in *Proc. Eur. Signal Processing Conf.*, Trieste, Italy, Sept. 10–13, 1996.

[15] D. F. Specht, "Probabilistic neural networks," *INNS Neural Networks*, vol. 3, no. 1, pp. 109–118, 1990.

[16] L. Hong, Y. Wan, and A. K. Jain, "Fingerprint image enhancement: Algorithm and performance evaluation," *IEEE Trans. Pattern Anal. Machine Intell.*, vol. 20, pp. 777–789, Aug. 1998.

[17] Y. Hamanato, "A Gabor filter-based method for fingerprint identification," in *Intelligent Biometric Techniques in Fingerprint and Face Recognition*, L. C. Jain, I. Halici, I. Hayashi, S. B. Lee, and S. Tsutsui, Eds. Boca Raton, FL: CRC, 1999, ch. 4, pp. 137–151.

[18] A. Erol, U. Halici, and G. Ongun, "Feature selective filtering for ridge extraction," in *Intelligent Biometric Techniques in Fingerprint and Face Recognition*, L. C. Jain, U. Halici, I. Hayashi, S. B. Lee, and S. Tsutsui, Eds. Boca Raton, FL: CRC, 1999, pp. 195–215.